Acta Biomaterialia 157 (2023) 137–148

Contents lists available at ScienceDirect

Acta Biomaterialia

journal homepage: www.elsevier.com/locate/actbio

Full length article

3D printed multi-growth factor delivery patches fabricated using dual-crosslinked decellularized extracellular matrix-based hybrid inks to promote cerebral angiogenesis

Seung Hyeon Hwang[a,1], Jongbeom Kim[b,1], Chaejeong Heo[c], Jungbin Yoon[a], Hyeonji Kim[a], Se-Hwan Lee[b], Hyung Woo Park[d,e], Man Seung Heo[d,e], Hyo Eun Moon[d,e], Chulhong Kim[a,b,f,g,h,*], Sun Ha Paek[d,e,*], Jinah Jang[a,b,g,h,*]

[a] Department of Mechanical Engineering, Pohang University of Science and Technology (POSTECH), 77 Cheongam-Ro, Nam-Gu, Pohang 37673, Republic of Korea
[b] Department of Convergence IT Engineering, Pohang University of Science and Technology (POSTECH), 77 Cheongam-Ro, Nam-Gu, Pohang 37673, Republic of Korea
[c] Center for Integrated Nanostructure Physics (CINAP), Institute for Basic Science (IBS), Suwon 16419, Republic of Korea
[d] Department of Neurosurgery, Cancer Research Institute, Ischemia/Hypoxia Disease Institute, Seoul National University, College of Medicine, Seoul 03080, Republic of Korea
[e] Advanced Institute of Convergence Technology, Seoul National University, Suwon 16229, Republic of Korea
[f] Departments of Electrical Engineering, and Medical Device Innovation Center, Pohang University of Science and Technology (POSTECH), 77 Cheongam-ro, Nam-gu, Pohang 37673, Republic of Korea
[g] School of Interdisciplinary Bioscience and Bioengineering, Pohang University of Science and Technology (POSTECH), 77 Cheongam-Ro, Nam-Gu, Pohang 37673, Republic of Korea
[h] Institute for Convergence Research and Education in Advanced Technology, Yonsei University, 50 Yonsei-ro, Seodaemun-gu, Seoul 03722, Republic of Korea

ARTICLE INFO

Article history:
Received 6 May 2022
Revised 4 November 2022
Accepted 23 November 2022
Available online 30 November 2022

Keywords:
Tissue engineering
3D printing technology
Dual-crosslinking decellularized extracellular matrix hydrogel
Drug delivery system
Cerebral angiogenesis

ABSTRACT

Generally, brain angiogenesis is a tightly regulated process, which scarcely occurred in the absence of specific pathological conditions. Delivery of exogenous angiogenic factors enables the induction of desired angiogenesis by stimulating neovasculature formation. However, effective strategies of mimicking the angiogenesis process with exogenous factors have not yet been fully explored. Herein, we develop a 3D printed spatiotemporally compartmentalized cerebral angiogenesis inducing (SCAI) hydrogel patch, releasing dual angiogenic growth factors (GFs), using extracellular matrix-based hybrid inks. We introduce a new hybrid biomaterial-based ink for printing patches through dual crosslinking mechanisms: Chemical crosslinking with aza-Michael addition reaction with combining methacrylated hyaluronic acid (HAMA) and vascular-tissue-derived decellularized extracellular matrix (VdECM), and thermal crosslinking of VdECM. 3D printing technology, a useful approach with fabrication versatility with customizable systems and multiple biomaterials, is adopted to print three-layered hydrogel patch with spatially separated dual GFs as outer- and inner-layers that provide tunable release profiles of multiple GFs and fabrication versatility. Consequently, these layers of the patch spatiotemporally separated with dual GFs induce excellent neovascularization in the brain area, monitored by label-free photoacoustic microscopy *in vivo*. The developed multi-GFs releasing patch may offer a promising therapeutic approach of spatiotemporal drugs releasing such as cerebral ischemia, ischemic heart diseases, diabetes, and even use as vaccines.

Statement of significance

Effective strategies of mimicking the angiogenesis process with exogenous factors have not yet been fully explored. In this study, we develop a 3D printed spatiotemporally compartmentalized cerebral angiogenesis inducing (SCAI) hydrogel patch, releasing dual angiogenic growth factors (GFs) using extracellular matrix-based hybrid inks. We introduce a new hybrid biomaterial-based ink through dual crosslink-

* Corresponding authors.
E-mail addresses: chulhong@postech.edu (C. Kim), paeksh@snu.ac.kr (S.H. Paek), jinahjang@postech.ac.kr (J. Jang).
[1] These authors contributed equally to this work.

https://doi.org/10.1016/j.actbio.2022.11.050

ing mechanisms: Chemical crosslinking with aza-Michael addition, and thermal crosslinking. 3D printing technology is adopted to print three-layered hydrogel patch with spatially separated dual GFs as outer- and inner-layers that provide tunable release profiles of multiple GFs and fabrication versatility. Consequently, these layers of the patch spatiotemporally separated with dual GFs induce excellent neovascularization in the brain area, monitored by photoacoustic microscopy *in vivo*.

1. Introduction

An angiogenesis of a brain is a tightly controlled process [1]. In general, blood vessels are hardly formed in the mature brain, unless under specific pathological conditions (e.g. hypoxia/ischemia) [1,2]. Meanwhile, a transient ischemic attack (TIA), a brief episode of brain dysfunction with clinical symptoms typically lasting less than one hour and without infarction, has a high possibility of proceeding to a permanent cerebral ischemia (i.e. ischemic stroke) [3–6]. Previous studies have shown that even though without current infarction in brain, the early implementation of secondary stroke prevention strategies, such as inducing angiogenesis, anticoagulation, and stents implantation, reduce the risk of stroke after TIA up to an 80% [6–9]. Among them, the induction of angiogenesis, which have evaluated to have better prognosis [10], serves to restore oxygen and nutrient supply needed for cellular infiltration and metabolic support [11,12]. Since the angiogenesis requires a complex and multi-step process with timely essential various angiogenic growth factors (GFs), the exogenous administration of angiogenic GFs could also effectively regulate the angiogenesis mechanism [11–14]. Thus, the delivery of exogenous angiogenic GFs have been emerging as a promising strategy for inducing blood vessels formation [15].

The angiogenic GFs that promote the initial and maturation phases of angiogenesis have been well identified [14,16]. The co-administration of pro-angiogenic factors of each phase has also been recognized as a beneficial method to promote regeneration of the blood vessels [11,17-21]. In particular, vascular endothelial growth factor (VEGF) is one of the critical factors for promoting the initial phase of angiogenesis and proliferating the endothelial cells to induce immature vessel sprouts. However, concerns about the clinical usage of VEGF have been raised due to the adverse effects of VEGF, such as pro-inflammatory response that includes increased vascular permeability [11]. Hepatocyte growth factor (HGF)—another significant angiogenic factor that promotes the maturation phase of angiogenesis—plays synergistic effects with VEGF via decreasing side effects of VEGF and promoting vascular endothelial cells. Thus, this sequential process can induce more robust angiogenic responses through prevention of vessel regression or formation of the leaky vessels [11,12]. Therefore, consecutive administration of these multiple pro-angiogenic factors, following the process of native angiogenesis mechanism, is imperative for promoting blood vessels formation effectively [18,22-24].

However, the conventional use of exogenous GFs, usually administrated by intravenous injections, is stunted by both safety and efficacy concerns. High dosages or repeated delivery are often required to achieve a desired effect, which results in several side effects and lower the efficacy [25–28]. Effectively inducing angiogenesis by administrating the angiogenic factors in a manner of physiologically proper times (temporal modulation) and at the proper site (site-specific spatial modulation) targeting remain imperative challenges for engineered drug delivery platforms [29]. Thus, it is necessary to develop a hydrogel patch-type drug delivery system having the tunable release profiles of angiogenic factors, while with soft and flexible properties for the local application in the delicate and fragile brain area.

To fabricate the patch, 3D printing technology could be adopted due to its versatility for manufacturing controllable and customizable patch-type delivery systems in a single and successive process using various types of biomaterials [30–32]. Many printing parameters (e.g., dimensions and design of the system) and material properties (e.g., synthetic and naturally-derived biomaterials, crosslinking density, and concentration) can be implemented with a desired shape to customize the release profiles [33–36]. As for the biomaterials, tissue-mimetic decellularized extracellular matrix (ECM)-based hydrogels and hyaluronic acid (HA, also an ECM-based hydrogel as a major component of brain ECM), which affects angiogenesis [37,38], have been suggested as a viable option [30,31,39]. Particularly, we recently demonstrated a vascular tissue-derived decellularized extracellular matrix (VdECM) with capability as a drug delivery carrier. However, the deficiency of printability of single VdECM has made it a challenge to be used as a printable biomaterial ink [29,40,41].

Herein, we fabricated a spatiotemporally compartmentalized cerebral angiogenesis inducing (SCAI) hydrogel patch using a biocompatible and biodegradable ECM-based hybrid hydrogel ink [42,43] with 3D printing technology for printing sophisticated and spatiotemporally separated patch at once with capability of sequential and sustained release of dual angiogenic GFs (Fig. 1). To develop the biomaterial ink, we used an effective chemical crosslinking mechanism at mild conditions, named as aza-Michael addition reaction, to promote the printability of VdECM ink through combining with methacrylated hyaluronic acid (HAMA). Methacrylates (Michael acceptors) in HAMA and amines (Michael donors) in VdECM undergo chemical reaction to form a hybrid ink (HAVEM ink). The aza-Michael addition reaction is an ideal mechanism for fabricating SCAI patch owing to the unnecessary of exogenous catalysts and the facilitating to tailor the printability and release profile of angiogenic GFs by simply changing the chemical crosslinking density. Using two types of HAVEM inks with different chemical crosslinking densities, we were able to fabricate a structure with spatially separated outer and inner layer by 3D printing technique. In addition, we investigated the efficacy for the combination of both GFs (VEGF and HGF), enabling the mimicking of angiogenesis for synergistically inducing more robust blood vessels. Therefore, the outer layer of the SCAI patch was printed with the initial early angiogenic factor VEGF laden HAVEM ink with lower chemical crosslinking density. Moreover, the inner layer was printed using the late angiogenic factor HGF laden HAVEM ink with higher chemical crosslinking density. After printing, the vitrification process to the SCAI patch was applied to make a thin, soft, flexible, and easily manipulable patch for grafting at the brain site. The superior *in vitro* and *in vivo* efficacy for the promoted neovascularization were demonstrated for the SCAI patch-based approach. We particularly observed time-dependent angiogenesis behaviors of cerebral microvessels for 14 days after implantation using a label-free, optical-resolution photoacoustic microscopy (OR-PAM) system [44–50]. The quantified results showed significant neovascularization performance at the brain site. Our dECM based hydrogel patch type approach with spatiotemporally separated dual GFs leads to excellent neovascu-

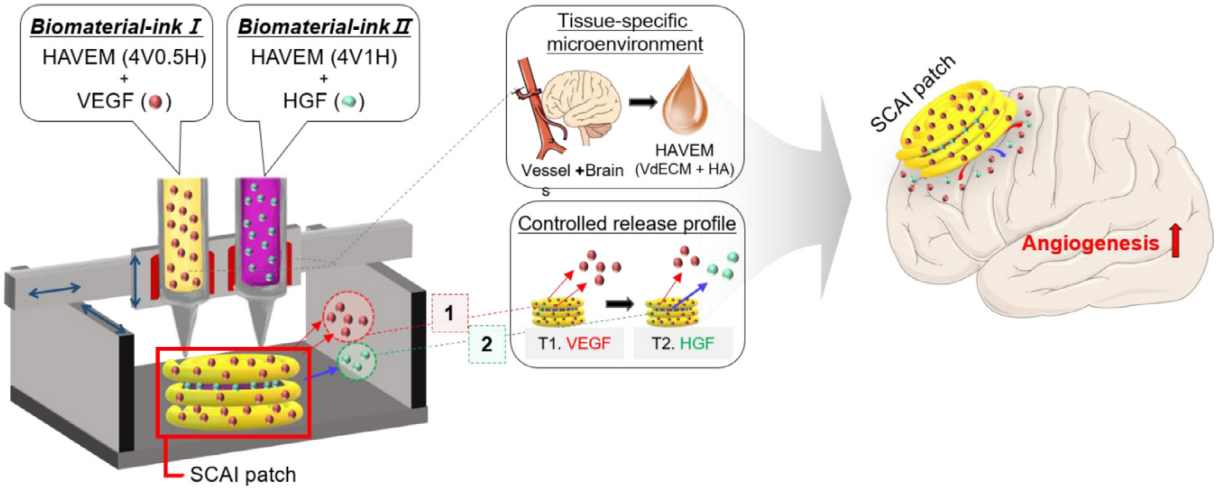

Fig. 1. Schematics of fabricating SCAI patches with dual crosslinked hybrid ink composed of VdECM and HAMA (HAVEM ink). Printing process was performed using HAVEM ink with regulating chemical crosslinking density to fabricate SCAI patch. SCAI patch sustained and sequentially releases VEGF and HGF that could promote brain angiogenesis.

larization in the brain area, and it could potentially contribute to clinical studies in ischemic diseases requiring induction of the angiogenesis.

2. Materials and methods

2.1. Preparation of VdECM ink

Vascular tissue was decellularized according to the previously reported protocol with minor adjustments [40]. In brief, the fresh porcine aortas were collected from a nearby slaughterhouse. The aorta tissues were stored at −80 °C or minced to cubic pieces of almost 2 mm in length, followed by washing with deionized water for 6 h to remove any remaining blood. The sliced pieces were then sequentially stirred in 0.3 wt% sodium dodecyl sulfate (Bioshop, Canada) solution for 24 h and then in 3 wt% Triton X-100 (Biosesang, Korea) solution for 24 h. After washing out the chemical detergents through rinsing with phosphate buffered saline (PBS) for 24 h, the tissues were treated with a nuclease solution of 75 U mL^{-1} DNase (Sigma-Aldrich, USA) and 50 mM $MgCl_2$ (Sigma-Aldrich, USA) solution in PBS at 37 °C for 24 h. The decellularized tissues were then sterilized using 0.1% peracetic acid solution (Tae-Sung international, Korea) in 4% ethanol (Samchun, Korea) for 4 h followed by rinsing several times with deionized water and PBS solution. Subsequently, the obtained VdECM was deep frozen at −80 °C and lyophilized for 48 h. For the preparation of VdECM biomaterial ink, the VdECM granules were dissolved in 7.5 mL 0.5 M acetic acid solution (Sigma-Aldrich, USA) with 15 mg of pepsin (Sigma-Aldrich, USA) for 100 mg VdECM for 48 h with strong stirring (at approximately 120 rpm). The undigested particles were removed by filtering VdECM solution through a 40 μm pore size mesh filter. Finally, the pH of VdECM solution was neutralized to 7.4 through dropwise addition of 10 M sodium hydroxide solution (Biosesang, Korea) on ice.

2.2. Preparation of HAVEM ink

We used two different compositions of hybrid inks to produce SCAI patches (Table 1). The aza-Michael addition reaction between HAMA (Advanced Biomatrix, USA) and VdECM produced a hybrid ink, named as HAVEM ink. To prepare HAVEM ink, VdECM and HAMA were mixed in neutral condition of pH 7 and kept at 4 °C for 10–12 h. Afterward, each growth factor of VEGF or HGF was mixed at a concentration of 0.05 μg μL^{-1} to the pre-crosslinked HAVEM inks to fabricate SCAI patches.

Table 1
Compositions of two hybrid biomaterial inks prepared for printing SCAI patches.

Composition of HAVEM inks		
	VdECM (w/v%)	HAMA (w/v%)
4V0H ink	4	0
HAVEM ink(4V0.5H)	4	0.5
HAVEM ink(4V1H)	4	1

2.3. Preparation of SCAI hydrogel patch

To develop releasing platform for the spatiotemporal compartmentalized dual growth factors, 3-layered round patch type hydrogel scaffolds were fabricated. The first, the second-outer, and the third layers were printed using HAVEM ink mixed with 0.05 μg μL^{-1} VEGF (recombinant human VEGF 165, PeproTech, USA). The second-inner layer was printed using HAVEM ink mixed with 0.05 μg μL^{-1} HGF (recombinant human HGF, PeproTech, USA). Two types of HAVEM ink were placed into each 24 G plastic nozzle-mounted 3-mL syringe (Musashi Engineering Company, Japan), which were then loaded into a multi-head 3D printing system (T&R Biofab, Korea). Under controlled temperature of 4 °C, all the three layers were printed in a spiral shape according to a programmed g-code. After printing each layer, a 20-second pause and 200-μm raise in Z-axis direction were applied were given to prevent mixing between the stacked layers.

2.4. Fabrication of vitrified SCAI patch

The printed 3-layered round SCAI patch was placed in an incubator for 1 h at 37 °C in 5% CO_2 environment for gelation process. Thereafter, SCAI gel-patch was dried for 10–12 h under air-ventilated conditions. The vitrified SCAI patches were used for *in vitro* and *in vivo* studies.

2.5. Physicochemical characterization of SCAI patch

Rheological analysis of each prepared biomaterial ink was conducted using Discovery Hybrid Rheometer-2 (TA Instruments, USA) system with a 20-mm cone plate geometry. The pH-neutralized three products of: (1) 4V0H ink; (2) 4V0.5H HAVEM ink; and (3) 4V1H HAVEM ink were prepared in solution state. Shear viscosity values were determined at an increasing shear rate from 0.01 to

1000 s^{-1} at 4 °C to evaluate the flow behavior of each biomaterial ink. The gelation kinetics of each product was examined in the oscillatory temperature sweep mode from 4 to 37 °C at a heating rate of 5 °C min^{-1}. To determine the frequency-dependent storage and loss moduli of biomaterial inks, a dynamic frequency sweep analysis in the range of 0.1–100 rad s^{-1} was also performed at 2% strain condition after incubation of the samples at 37 °C for gelation. All experiments were performed and data were analyzed in triplicate. To verify the chemical crosslinking reaction via aza-Michael addition reaction, the lyophilized samples were dissolved in D_2O and ^1H NMR (400 MHz) spectra were recorded on a Bruker Advance III HD 400-MHz NMR spectrometer. Afterward, the tensile properties were examined using an MTS extensometer (AVX54, MTS). To prevent slipping, the rectangular-shaped vitrified patch samples (25 mm × 8 mm × 400 μm) were prepared and fixed by means of a screw-grip mounted to the MTS extensometer.

2.6. Growth factors releasing examination

Recombinant human VEGF 165 (100–20, PeproTech, USA) and recombinant human HGF (100–39H, PeproTech, USA) were encapsulated in each ink at a final concentration of 0.05 μg μL^{-1}. Then, they were subjected to two-step crosslinking and physical separation during SCAI patch fabrication steps. Vitrified disk-shaped (8 mm in diameter and 250 μm in height) SCAI patch was immersed in 1.1 mL of PBS at 37 °C. In the next step, 1 mL of the solution was harvested and stored at –80 °C on each pre-determined time points while the same volume of PBS was replaced. We used ELISA kits specific to determine VEGF (DY293B, R&D systems, USA) and HGF (DY294, R&D systems, USA) according to the manufacturer's instructions to quantify the released growth factors from each patch. All samples were examined and analyzed in triplicate.

2.7. In vitro *characterization of SCAI patch*

Human brain microvascular endothelial cells (HBMECs; Innoprot, Korea) were cultured using an endothelial cell medium kit (ECM; Innoprot, Korea) supplemented with 5% (v/v) fetal bovine serum, 1% (v/v) endothelial cell growth supplement, and 1% (v/v) penicillin/streptomycin solution and incubated at 37 °C in 5% CO_2 environment while the media changing in every two or three days. Once the confluence reached 90%, the cells were washed with Dulbecco's PBS and detached through incubating with 0.25% Trypsin-EDTA (Gibco, USA) for 4 min at 37 °C in 5% CO_2 environment.

Tube formation assay was performed according to the manufacturer's instructions. Briefly, on the day of the assay, 10 μL of matrigel (Corning) was added to the ibidi μ-Slide Angiogenesis dish (ibidi, Germany) and incubated for 1 h at 37 °C with 5% CO_2. During the incubation time, HBMECs were harvested. The cells were counted and 50 μL of cells suspension containing 5000 cells with each growth factors of VEGF and HGF at a final concentration of 0.05 μg μL^{-1} were added to the wells containing the matrigel. The slides were then incubated at 37 °C for 48 h. The formed tubes were visualized and captured by live-cell imaging mode using a fluorescence microscope (Nikon Instruments, Japan). Tube formation was quantified through measurement of the total tube length using ImageJ software.

To evaluate *in vitro* cell viability and cytotoxicity, 2×10^4 HBMECs were added into each well of a 12-well cell culture plate while vitrified SCAI patches were placed in the transwell inserted to each well. Cells were incubated for 7 days at 37 °C and 5% CO_2 and then dyed with a live/dead assay kit (LIVE/DEAD Cell Viability Assay, Thermo Fisher Scientific, USA) following the manufacturer's instructions. Live and dead cells were visualized in green and red, respectively, under a fluorescence microscope (Nikon Instruments, Japan). The cell proliferation was quantified using the cell counting kit-8 assay kit (Cell Counting Kit-8, Dojindo Molecular Technologies, Japan) following manufacturer's protocol. Briefly, the cells on the wells were cultured with CCK-8 solution at a 1:10 dilution with fresh medium for 3 h at 37 °C. The solutions were transferred in triplicate to an optically clear 96-well flat bottom plate. Absorbance at 450 nm was measured using Multiskan GO microplate spectrophotometer (Thermo Fisher Scientific, USA).

Table 2
Primer sequence for quantitative real-time PCR analysis.

Gene		Sequence
hu-GAPDH	Forward	5′-CAATGACCCCTTCATTGACC-3′
	Reverse	5′-GACAAGCTTCCCGTTCTCAG-3′
hu-FLT1	Forward	5′-CACCCAGCACATCATGCAA-3′
	Reverse	5′-TTCCCCCCTGCATTGGA-3′
hu-FLK1	Forward	5′-ATTCCTCCCCCGCATCA-3′
	Reverse	5′-GCTCGTTGGCGCACTCTT-3′
hu-ANGPT1	Forward	5′-GCGGGACAAAACCATGGA-3′
	Reverse	5′-AACTGGGCCCTTTGAAGTAGTG-3′
hu-PECAM	Forward	5′-TATGATGCCCAGTTTGAGGT-3′
	Reverse	5′-GAATACCGCAGGATCATTTG-3′

2.8. Quantitative real-time PCR analysis

The HBMEC samples were cultured on 12-well plates with 2 kinds of patches (SCAI patches without exogenous GFs and SCAI patches) placed on transwell (Corning, USA) at a density of 1.5×10^4 cells per well in 1.5 mL of ECM medium. On culture days of 3, 7, and 14, mRNA on the well was extracted using RNAisoplus (Takara Bio, Japan). The RNA concentration and its purity were determined with Nanodrop Lite spectrophotometer (Thermo Fisher Scientific, USA). Afterward, reverse transcription was performed using the SuperScript IV First-Strand Synthesis System (Invitrogen Life Technologies, USA). Real-time PCR was performed using StepOne Plus Real-Time Cycler (Applied Biosystems, USA) with SYBR-green I reagent (Takara Bio, Japan). Data were analyzed using StepOne software v2.3 and expression levels of each gene normalized to GAPDH expression were calculated according to the $2^{-\Delta\Delta CT}$ method. The primer sequences were designed based on published gene sequences on the NCBI and PubMed (Table 2). Each group was tested in triplicate.

2.9. Preparation and procedure of in vivo *study of SCAI patch*

All animal studies were performed according to the guidelines of national regulations with the approval of the local Institutional Animal Care and Use Committee (POSTECH-2021–0022). Eight-week-old weighing 200–300 g male Sprague-Dawley (SD) rats were used for *in vivo* experiments. All experiments were performed on experimental animal of at least four in each groups, a total of 8 animals. The anesthesia of rats was performed using an induction chamber with 4.0% isoflurane at first and then maintained with 1.5% of isoflurane during surgery. Their heads were firmly fixed with ear bars in a stereotaxic frame, and the body temperature was maintained with a heating pad. After shaving the head, incision was made over the scalp of the hemisphere. The remaining epidermis and debris were removed with saline. A craniotomy was then carefully performed using a dental drill. The skull between bregma and lambda was removed in an oval shape of about 6 mm x 5 mm. The end of the 6 mm diameter SCAI patch was slightly folded and implanted on the exposed dura matter. The 6 mm diameter SCAI patch was then implanted on the exposed brain tissue. Then, an oval-shaped polydimethylsiloxane (PDMS) membrane with a size of 8 mm × 7 mm and thickness of approximately 150 μm, which was sterilized and soaked in a saline fully covered the exposed brain site. The boundary of the

PDMS membrane was sealed onto the skull using cyanoacrylate glue (Loctite, USA). Thereafter, a dental resin (OA2, Denkist Inc., Korea) was applied along the edges of the PDMS membrane and exposed to UV light for 15 s for permanent implantation within the skull. Finally, the rats were administered Baytril (5 mg kg^{-1}, Bayer, Germany) via subcutaneous injection and returned to their cages. Subsequently, Tylenol (0.5 mg mL^{-1}, Janssen, Korea) and Marboxyl (0.06 mg mL^{-1}, Vetoquinol, Korea) were provided in the drinking water to relieve inflammation [51]. In the post-operative 2 weeks, the brain sites were monitored using OR-PAM system. Afterward, the brain tissues were harvested and analyzed using hematoxylin and eosin (H&E) staining and immunohistochemistry (IHC) to evaluate the functional angiogenic efficacy of SCAI patch.

2.10. In vivo *time-dependent photoacoustic monitoring of cerebral angiogenesis derived via SCAI patch*

We used an OR-PAM system (OptichoM, Opticho, Korea) to monitor brain angiogenesis [52,53]. OR-PAM is the premier *in vivo* imaging tool for non-invasive exploration of volumetric microvasculature. The OR-PAM system uses a nano-pulse laser system (VPFL-G-10, Spectra-Physics, USA) with a wavelength of 532 nm, which is well absorbed by a red blood cell to generate ultrasound waves from the blood vessels.

The generated ultrasound waves were measured with a custom-made ultrasound transducer at a central frequency of 20 MHz and a bandwidth of 60%, which has a theoretical axial resolution of 113 μm. We reconstructed a wide field of view (FOV) image through assembling segmented images. The segmented images were acquired with a galvanometer scanner (GVS001, Thorlabs, USA) and two linear motorized stages (L-509.10SD00, Physik Instrumente, Germany). A galvanometer scanner and a linear stage were used to obtain a segmented image. The galvanometer scanner steers laser pulses at a scanning range length of 1.6 mm (with 400 pixels) and with a scanning speed of 50 Hz. A linear motorized stage with a maximum scanning range of 26 mm (with a step size of 5 μm) moves the scanning part of the OR-PAM system in a direction perpendicular to the scanning direction of the galvanometer scanner. The scanning range of the stage was adjusted according to the size of ROI. The other linear stage enables to provide segmented images from other regions by moving the scanning part in the same scanning direction as of the galvanometer scanner. The obtained segmented images were reconstructed into a wide FOV image by a structural similarity (SSIM)-based volumetric image registration algorithm using a pyramid blending [52,54].

To quantify newly formed blood vessels in a photoacoustic (PA) image, we compared the ratio of the area of blood vessels with a diameter of smaller than 50 μm to the area of ROI with the skull removed. To calculate the blood vessel density, first, a mask was created to remove the region outside of the ROI, and then the blood vessels larger than approximately 150 μm in diameter were removed from the PA maximum amplitude projection (MAP) image of the rat brain. The area of the ROI was calculated with the area of the mask. Next, after application of the hessian-based vessel filter [55], we extracted blood vessels with diameters of 50 μm or larger from the filtered image and made a large vessel map based on the extracted blood vessels. Finally, we subtracted the large vessel map from the vessel-filtered image to reconstruct the small vessel map with vessels smaller than 50 μm in diameter and calculated the area of the small vessels based on the small vessel map.

2.12. Histological analysis

After harvesting the brain, the samples were fixed in 4% paraformaldehyde solution and sectioned at the region of the surgery part where the patch was attached. The paraffin-embedded samples were transversely sectioned at thickness of 3 μm for H&E staining experiments. The stained images were digitally archived using a microscopy system (Leica DM750, Leica, Germany).

2.13. Immunohistochemistry

Tissue samples fixed in 4% paraformaldehyde- solutions were embedded in paraffin and sectioned in 3 μm thickness for immunofluorescence examinations. Deparaffinization and rehydration steps were performed using antigen retrieval with a buffer. The sections were incubated in 3% hydrogen peroxidase solution for 10 min at room temperature and stained with primary antibodies against CD31 (1:1000, abcam, UK). The stained sections were further incubated with peroxidase-conjugated secondary antibodies (Envision+ Rabbit, DAKO, USA) for 30 min and applied Mayer's Hematoxylin for counterstaining. The obtained slides were visualized under a microscopy system (Leica DM750, Leica, Germany).

2.14. Statistical analysis

All data were provided as mean ± standard error of the mean (SEM) and all statistical analyses were performed using GraphPad Prism 8.2.1 program (GraphPad Software, USA). Significance of differences between data were assessed via two-way ANOVA or *t*-test. The representation of statistical significance is as follows: $^{*}p < 0.05$, $^{**}p < 0.01$, $^{***}p < 0.001$, $^{****}p < 0.0001$.

3. Results

3.1. Development and physicochemical properties of HAVEM ink

To accomplish a programmed loading and releasing of angiogenic factors from the patch, we developed a novel dual-crosslinked hybrid biomaterial-based ink via synthesizing HAMA and VdECM, named as HAVEM ink. Since HAVEM inks could be synthesized by various combinations of VdECM and HAMA ratio, HAVEM inks synthesized by 4% VdECM with 0.5% HAMA, and 4% VdECM with 1% HAMA were named 4V0.5H, and 4V1H, respectively. For the HAMA, two distinct chemical and thermal crosslinking (gelation) mechanisms were involved during pre- and post-printing processes, respectively (Fig. 2(A)). First, the chemical crosslinking process of the HAVEM ink occurred between methacrylates of HAMA and amines of VdECM via aza-Michael addition reaction. Chemical bonds formed via aza-Michael addition reaction were verified using NMR spectroscopy (Fig. 2(B) and Figure S1). The NMR spectrum of HAMA shows the NMR characteristic peaks of methacrylate group at 1.9, 5.7, and 6.1 ppm [56], while these peaks were not observed in the spectrum of the ink containing only VdECM (4V0H) at the same positions, indicating the absence of the methacrylate group. Moreover, the NMR characteristic peaks were also not observed in the HAVEM ink groups (4V0.5H and 4V1H), specifying that all methacrylate groups in HAMA successfully reacted and formed chemical crosslinking in reaction with the amine groups of VdECM. After, in the post-printing process, thermal crosslinking occurred in which the ECM-based ink crosslinked at 37 °C to form a gel [57].

Meanwhile, the chemical crosslinking density could be controlled by regulating the reaction ratio of each VdECM and HAMA. Then, the printability and mechanical properties of the HAVEM ink depending on the ratio of HAMA was confirmed. Both of the HAVEM inks with different chemical crosslinking densities (4V0.5H and 4V1H) exhibited a shear-thinning rheological behavior with slightly higher viscosity than the ink containing only VdECM (4V0H) (Fig. 2(C)). More specifically, as the chemical crosslinking density increased, the fluidity of inks decreased while their viscosity increased. While the viscosity of each HAVEM ink was hardly

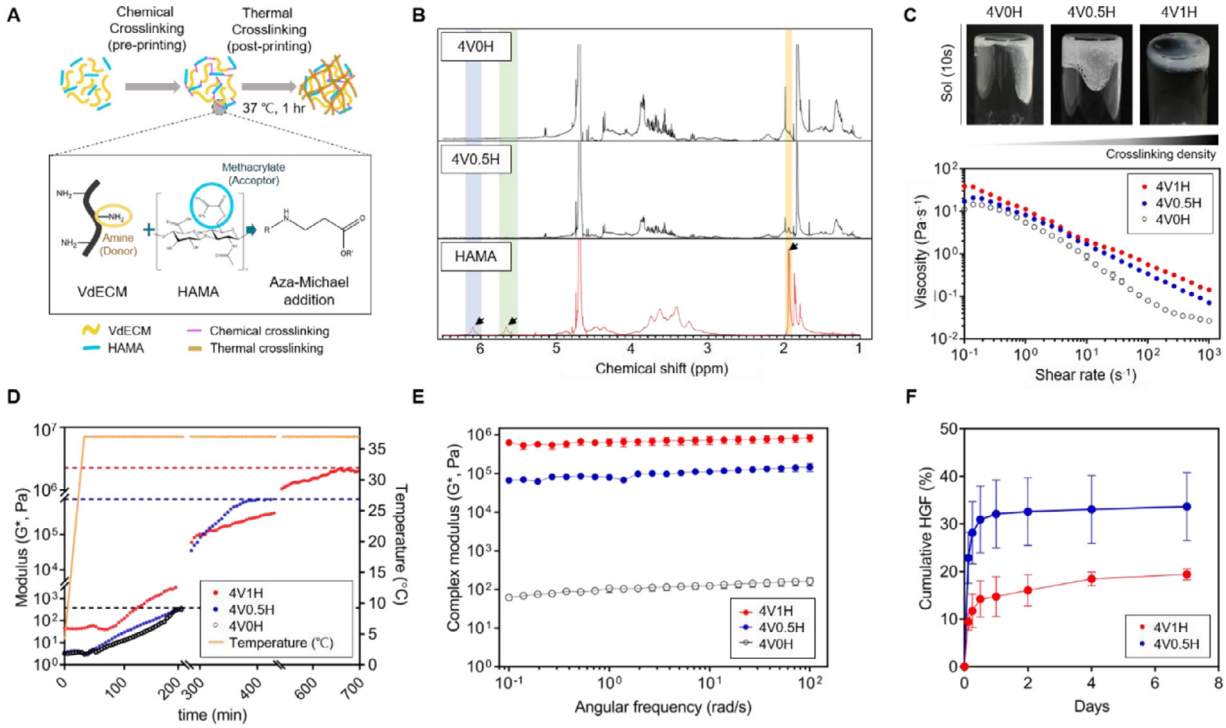

Fig. 2. Characteristics of HAVEM inks. (A) Schematic of dual crosslinking mechanism of HAVEM ink and mechanism of chemical crosslinking derived from aza-Michael addition reaction through synthesizing VdECM and HAMA. (B) Nuclear magnetic resonance (NMR) spectra for VdECM (4V0H), HAMA, and HAVEM (4V0.5H) ink to verify occurrence of crosslinking reactions. NMR characteristic peaks related to methacrylate group were highlighted at 1.9, 5.7, and 6.1 ppm. (C) Variations of viscosity at various shear rates at printing condition of 4 °C and sol state images for various combinations of HAVEM inks according to differences of chemical crosslinking density. Samples: 4V0H, 4V0.5H, and 4V1H. (D) Gelation kinetics represented by variation in modulus at temperatures from 4 to 37 °C. (E) Variation of dynamic modulus at various frequency at 37 °C. (F) Release profile of HGF encapsulated in 4V0.5H and 4V1H with ± SEM measured for 7 days. All experiments were performed in triplicate. (For interpretation of the references to colour in this figure legend, the reader is referred to the web version of this article.)

affected in the course of time after the chemical crosslinking reaction (Figure S2).

Whereas the mechanical properties of each of the inks (4V0H, 4V0.5H, and 4V1H) drastically changed after completing the dual crosslinking process. To verify the effects of the regulating crosslinking density on the mechanical characteristics, the changes in the complex moduli of fabricated inks were monitored while raising the temperature from 4 to 37 °C. As expected, the HAVEM ink containing higher HAMA concentration (4V1H) exhibited further increase in complex modulus as thermal crosslinking proceeded in comparison with that of the HAVEM ink containing lower HAMA concentration (4V0.5H) and VdECM alone (4V0H). Moreover, the time required to reach the plateau was observed relatively longer for 4V1H HAVEM ink than the other ones (4V0.5H, 4V0H) (Fig. 2(D)). It could be inferred that as the proportion of HAMA in the HAVEM ink increased, more chemical crosslinking occurred, resulting in a larger complex modulus. At plateau, the complex modulus of 4V1H ink was observed to be 1.91 times and 3045 times greater than those of the 4V0.5H and 4V0H inks, respectively (indicated by red, blue, and black dotted lines, respectively). Next, we verified the complex modulus of the gel-state inks after chemical and thermal crosslinking of HAVEM inks. The 4V1H ink also revealed the largest value of complex modulus followed by 4V0.5H and 4V0H inks. The observation indicates a robust structural fidelity of this hybrid inks depending on the pre-printing chemical crosslinking densities (Fig. 2(E) and Figure S3). Consequently, the desired mechanical properties were accomplished by changing the chemical crosslinking density in the HAVEM inks.

Furthermore, we exhibited that a chemical crosslinking density of each HAVEM ink had a direct impact on the release rate of angiogenic factor loaded in the ink (Fig. 2(F)). Two types of HGF-laden HAVEM inks, 4V0.5H and 4V1H, were used to verify the release rate of HGF from hydrogel made with each ink. We identified that HGF was released more slowly from the hydrogel fabricated with 4V1H ink, which had a higher chemical crosslinking density, than from the hydrogel fabricated with 4V0.5H. Thus, the results demonstrate that the higher the chemical crosslinking density, the slower GFs releasing rate, which indicates the chemical crosslinking density of HAVEM ink is one of the critical factors for controlling GFs releasing rate.

3.2. Design and fabrication of SCAI patch using 3D printing technology

We selected two types of HAVEM inks to fabricate the SCAI patches; 4V0.5H and 4V1H. The patch structure was designed and 3D printed in a three-layered round shape, compartmentalizing the outer and the inner layers. As the erosion occurs faster in the separated outer layer than in the inner layer, the loaded GFs on the outer layer could release faster [58]. On the outer layer, 4V0.5H HAVEM ink with lower chemical crosslinking density loaded VEGF (the angiogenic factor involved in the early phase of angiogenesis) was applied for early releasing, while on the inner layer, 4V1H HAVEM ink with higher chemical crosslinking density loaded HGF (the angiogenic factor for the later phase of the angiogenesis) was used for sustained releasing (Fig. 3(A)). The combination of these GFs effectively induced rapid and prolonged tube formation of human brain microvascular endothelial cells (HBMECs) and formed the greatest number of total tube length after 48 h compared with the group treated the single GFs (Figure S4). Consequently, VEGF-laden 4V0.5H HAVEM ink (Ink A) and HGF-laden 4V1H HAVEM ink (Ink B) were used to fabricate the 8-mm diameter SCAI patches. Initially, the first layer was printed using Ink A with 8 mm in diameter of spiral trace (Movie S1). For physically blocking the

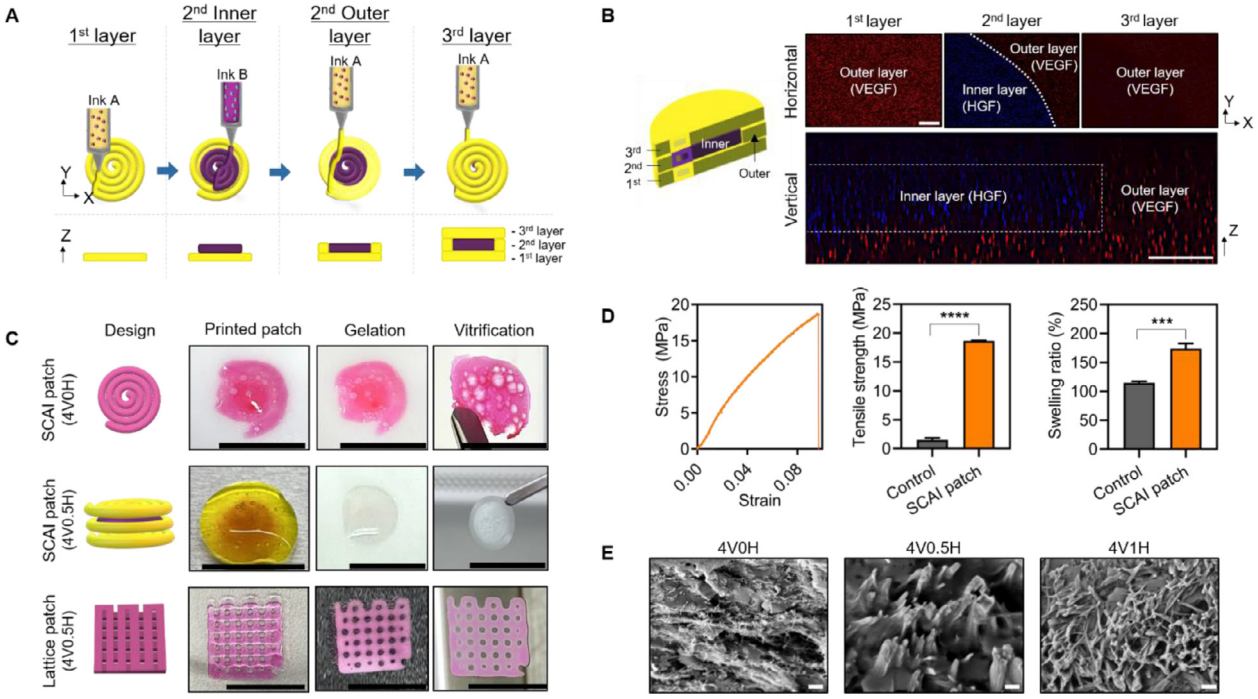

Fig. 3. Fabrication of triple-layered SCAI patch separated by dual HAVEM inks (4V0.5H and 4V1H) with different compositions of VdECM, HAMA and growth factors. (A) Schematics of fabricating SCAI patch using 3D printing technique to print triple-layered structures with dual growth factors of VEGF and HGF. (B) Confocal microscopy images of cross-section and each layer of patch structures (scale bars: 200 μm). (C) Fabricated versatile structures having various combinations of HAVEM ink and crosslinking with vitrification images of each structure. In Design 1 (upper row), spiral shape was printed using 4V0H ink; Design 2 (middle row), SCAI patch was printed using 4V0.5H ink in outer part and 4V1H ink in inner part; Design 3 (lower row), lattice shape was printed using 4V0.5H ink (scale bars: 10 mm). (D) Tensile strength examination results and swelling ratio for vitrified SCAI patch. (E) SEM micrographs of vitrified patch containing various inks of 4V0H, 4V0.5H, and 4V1H (scale bars: 1 μm). (For interpretation of the references to colour in this figure legend, the reader is referred to the web version of this article.)

HGF from the external area, the second-inner layer was printed with Ink B in diameter of 6 mm of the spiral trace with same center, followed by second-outer and third layers printing using Ink A in the same printing conditions. After printing each layer, a 20-second pause and 200-μm raise in Z-axis direction were applied. Thus, HGF was not only spatially compartmentalized through the printing process, but also temporally compartmentalized using 4V1H HAVEM ink, which prevented the release of HGF from the patch at the initial phase of the angiogenesis process. In this strategy, the core layer was printed with HGF-laden 4V1H HAVEM ink (Ink B), totally enclosed by the outer layers printed with VEGF-laden 4V0.5H HAVEM ink (Ink A). On the other hand, VEGF-laden 4V0.5H HAVEM ink (Ink A) was placed at all first and second-outer and third layers so that VEGF could immediately be released after grafting the patch to amplify the efficacy of inducing the initial angiogenesis process. This compartmentalized structure of the patch was well maintained after printing and post-printing thermal crosslinking process (Movie S2). The observation demonstrates excellent printability of HAVEM ink for producing the desired construct using a multi-material-based printing process (Fig. 3(B)). Indeed, 4V0H ink was not appropriate for printing the desired shape of the SCAI patch because of its relatively lower shape fidelity than that of the HAVEM ink (Fig. 3(C)). However, the HAVEM ink revealed versatility for fabrication. With this ink, not only the spiral-shaped SCAI patch, but also a double-layered lattice-shaped fine pore hydrogel construct was possibly fabricated.

After completing post-printing thermal crosslinking of the printed SCAI patch, a vitrification process was performed [59] to facilitate thin as a thickness of 130 ± 20 μm, easy handling and storage for the following grafting process during surgery due to increased mechanical properties (Movie S3). Tensile stress-strain properties were examined to evaluate mechanical properties of the SCAI patch after the vitrification process. The vitrified SCAI patch exhibited a tensile strength of 18.62 MPa, which was 12.46 times greater than that of the control sample without going through the vitrification process (Fig. 3(D)). The vitrified SCAI patch was rapidly rehydrated when immersed in a saline, resulting in a swelling ratio of up to 151%. The ultrastructure of the vitrified SCAI patch was evaluated using SEM technique, exhibiting interconnected and porous structures as the changing of the crosslinking densities (Fig. 3(E)). When the crosslinking density increased, the fibril density also increased [60]. This observation is clearly demonstrated in the SEM micrographs by showing the increasing fibril densities as the crosslinking densities increase, in the order of 4V0H, 4V0.5H, and 4V1H.

3.3. *Sustained and sequential release profiles of SCAI patches and* in vitro *cellular behaviors*

After characterization of SCAI patches, we investigated the release profiles of GFs from the fabricated patches. In order to sustained and sequentially release of VEGF and HGF, we adopted two strategies: Tailoring the chemical crosslinking density of HAVEM ink containing each GFs and using 3D printing technique to fabricate hydrogel patch having spatiotemporally separated two angiogenic factors.

Hydrogel with lower chemical crosslinking density contains more water, causing faster degradation of hydrogel, resulting in a rapid release of laden GF. Likewise, the higher chemical crosslinking density of hydrogel, the lower release rate for the GF [35]. As the SCAI patch was chemically crosslinked in a hydrophilic matrix, tailoring the chemical crosslinking density could regulate the degradation rate of the chemical bonds which can be considered as an erosion, result in control of the release profile of the embedded GFs [61].

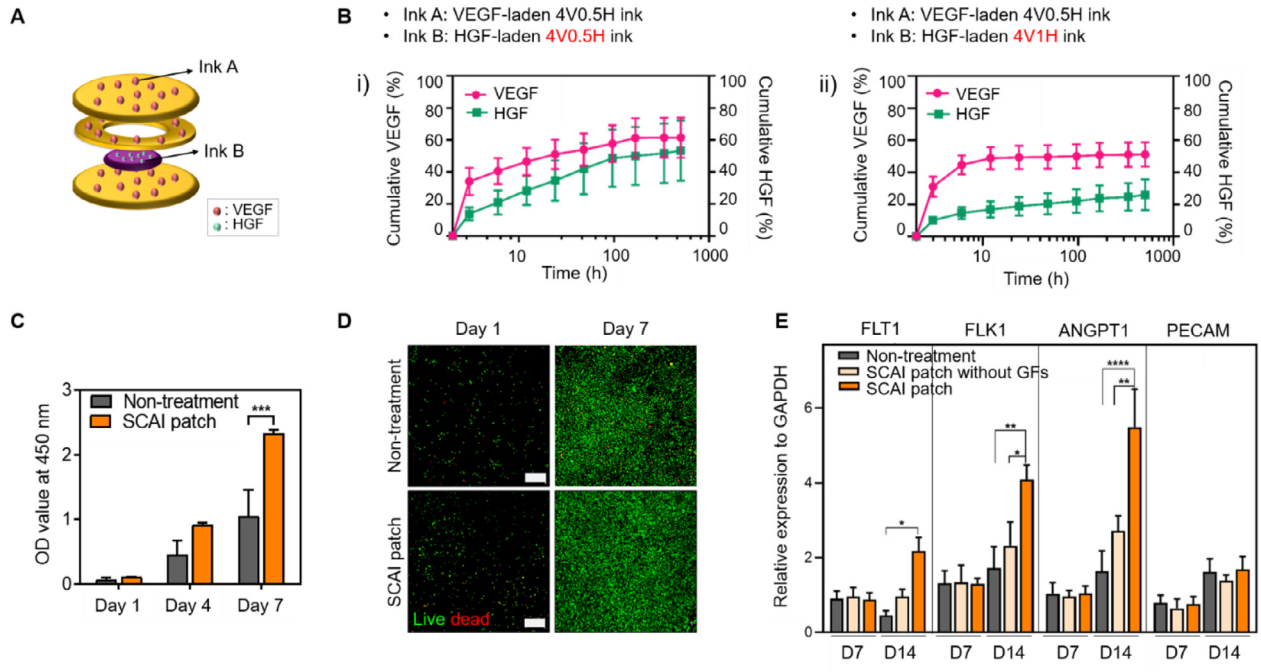

Fig. 4. Sustained sequential growth factors releasing kinetics of SCAI patch and *in vitro* experiments. (A) Illustration of multilayer SCAI patch designed for sequential drug release of VEGF and HGF. (B) Cumulative release profiles of VEGF and HGF in each type of the patches evaluated for a month. i) In left graph, HAVEM ink (4V0.5H) containing 0.05 μg μL^{-1} of VEGF was used for outer layer and HAVEM ink (4V0.5H) containing 0.05 μg μL^{-1} of HGF for inner layer; and ii) in right graph, HAVEM ink (4V0.5H) containing 0.05 μg μl^{-1} of VEGF was used for outer layer and HAVEM ink (4V1H) containing 0.05 μg μL^{-1} of HGF for inner layer. (C) *In vitro* HBMECs culture results. HBMECs were cultured with SCAI patch on transwell and cell proliferation analysis results of HBMECs within the SCAI patch obtained on days 1, 4, and 7. (D) Live/dead cell assay results for cell viability of HBMECs of SCAI patch on days 1, 4, and 7 (scale bars: 50 μm). (E) *In vitro* angiogenic gene expression results (PCR) on day 7 and day 14. (For interpretation of the references to colour in this figure legend, the reader is referred to the web version of this article.)

To validate our strategy designed for the sustained and sequential drug release of VEGF and HGF, we made two experimental groups based on the multilayer SCAI patches (Fig. 4(A) and (B)). In one group (i), a VEGF-laden 4V0.5H ink (Ink A) on the outer layer and HGF-laden 4V0.5H ink (Ink B) on the inner layer were used to fabricate patch. As each of the GFs were laden with the same 4V0.5H ink and only spatially compartmentalized, the efficacy of spatial separation on the sustained release of GFs could be verified (Fig. 4(B)). On the other hand, in another group (ii), SCAI patches were fabricated by using a VEGF-laden 4V0.5H ink (Ink A) on the outer layer and HGF-laden 4V1H ink (Ink B) on the inner layer. Two angiogenic factors, VEGF and HGF in the SCAI patch were temporally separated using HAVEM inks with different chemical crosslinking densities, and spatially compartmentalized using 3D printing technique. We could verify the efficacy of sustained and sequential release of dual GFs in spatiotemporally compartmentalized structures using these strategies.

As a result, for VEGF encapsulated in the outer layer of the patches in both groups, 50.07% ± 10.63% were released within a day (24 h) for both groups without any significant difference. On the other hand, in the case of HGF in both groups, since it was spatially separated and located in the inner layer, it could be relatively protected from erosion by the aqueous environment in both groups, which obviously showed sustained release kinetics compared with VEGF. Moreover, unlike group (i), in group (ii), ink conditions were also differentiated to separate GFs temporally, by using HAVEM inks with different chemical crosslinking densities in Ink A and Ink B, respectively. In group (ii), which had different chemical crosslinking densities of HAVEM inks used for the outer and inner layers, HGF encapsulated in the 4V1H of the inner layer showed a sustained release profile which took about 30 days to release approximately 50% of the initial loading amount, whereas the group (i) of HGF contained in the 4V0.5H ink of the inner layer, a similar amount of was released in just 4 days. Therefore, the data of group (ii), in which the growth factors were separated temporally and spatially, suggested significantly reinforced sustained and sequential release profile than group (i), which was separated only spatially.

For assessment of the potential of inducing angiogenesis, we examined cytocompatibility and biofunctionality of the SCAI patch *in vitro*. The patch did not show any deleterious effect on the cell viability when it was cultured with HBMECs for 7 days and promoted proliferation rate compared with that of the non-treatment group (Fig. 4(C)). This phenomenon was also cross validated using qualitative live/dead cell staining assay (Fig. 4(D)). In addition, the quantitative analyses of the expressions of angiogenesis-specific gene markers were performed to evaluate the cellular performance under the influence of the SCAI patch (Fig. 4(E) and Figure S5). At the early phase of angiogenesis, the SCAI patch-treated group did not reveal a significant difference in regulating gene expression involved in the angiogenesis than the non-treatment group and the SCAI patch without GFs group (day 3 and 7). As the phase of the angiogenesis progressed, the difference in expression levels of angiogenic gene of SCAI patch treated group showed increasing trend over time compared to the non-treatment group and the SCAI patch group without GF group (day 3, 7, and 14). The expressions of crucial angiogenic gene markers, including FLT1, FLK1, and ANGPT1, elevated in the patch implanted groups (SCAI patch group and SCAI patch without GFs group) after 14 days. Especially, the expressions of these genes showed a statistically increased in the SCAI patch implanted group after 14 days. With these results, it can be noted that the SCAI patch presents a strong influence on the upregulating the expressions of pro-angiogenic genes, particularly related to the neovessels maturation. The spatiotemporally sequen-

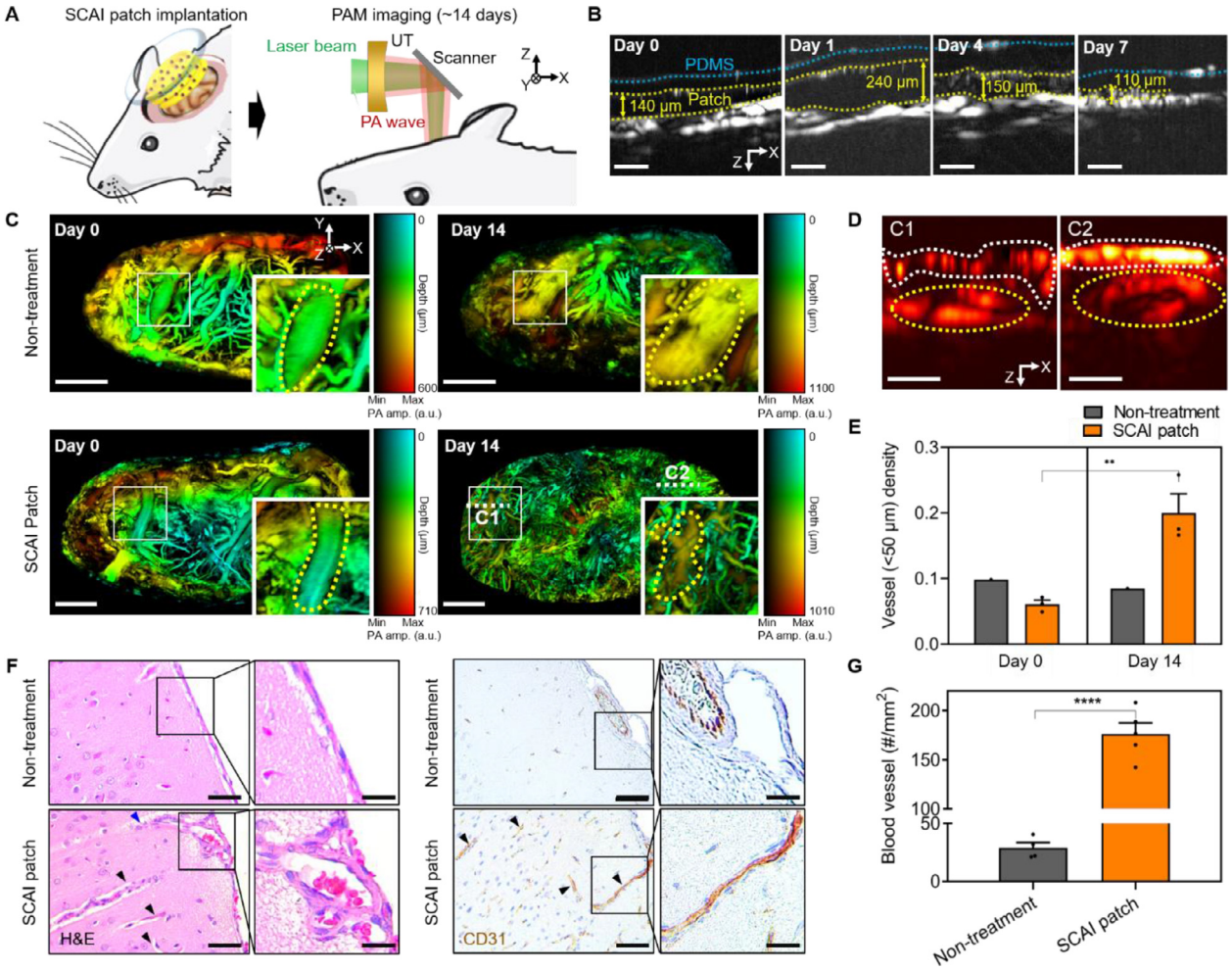

Fig. 5. Patch induced neovascularization *in vivo* experiments. (A) Schematics of *in vivo* experiment. After implanting a SCAI patch into cerebral cortex of a SD rat, the implanted region was monitored with OR-PAM for 14 days. (B) Variation of implanted SCAI patch thickness with cross-sectional PA B-mode images of patch-implanted region on days 0, 1, 4, and 7 (scale bars: 200 μm). (C) MAP images of cerebral vasculature of SD rats with and without an implanted SCAI patch on days 0 and 14. Large blood vessels are highlighted by yellow dotted lines in enlarged image (scale bar: 1 mm). (D) Cross-sectional PA B-mode images in regions of C1 and C2 white dotted lines of PA image obtained from rat with a SCAI patch in (C) (scale bar: 400 μm). White and yellow dotted curves include neovasculature and covered large blood vessels, respectively. (E) Quantitative analysis of blood vessel density with ± SEM using OR-PAM images. (F) H&E staining images and IHC images (CD 31) of non-treatment group and SCAI patches implanted group after 14 days (scale bars: 50 μm, for enlarged images, scale bars: 20 μm). (G) Blood vessel quantification with ± SEM using IHC images. (For interpretation of the references to colour in this figure legend, the reader is referred to the web version of this article.)

tial releasing of VEGF and HGF from the SCAI patch to the HBMECs mimics the angiogenesis process and synergistically induces effective angiogenesis compared to the SCAI patch without exogenous GFs.

3.4. In vivo *brain angiogenesis after implanting SCAI patches*

To evaluate the brain angiogenesis inducing potential *in vivo*, we used an OR-PAM system to visualize angiogenic behaviors of the cerebral blood vessels induced by the SCAI patch in a time-dependent manner (Fig. 5(A)). A cranial window was generated during craniotomy on rats in which the vitrified SCAI patch with a thickness of 130 ± 20 μm was implanted where the skull was removed, followed by covering with a transparent polydimethylsiloxane (PDMS) membrane with a thickness of approximately 150 μm to enable penetration of optical beams and PA waves for monitoring [51]. The regions of interest (ROI) of the rats were photoacoustically imaged for 14 days to monitor the blood circulation and changes in the cerebral cortex microvasculature. In order to compare the angiogenesis results for each group, we displayed representative images obtained by OR-PAM from the same mouse in the same area of interest with the skull removed.

The cross-sectional PA B-mode images were obtained from the implanted site to track the change in the SCAI patch over time (Fig. 5(B) and Figure S6). The boundaries of the patches were determined by weak PA signals generated from the translucent SCAI patch, highlighted by the yellow dotted lines. The thickness of the patch was measured as 140 μm on day 0, similar to that of the vitrified SCAI patch. The thickness of the swelled patch increased up to 240 μm after one day of implantation and then gradually degraded until approximately 110 μm on day 7. After 14 days of implantation, the patch was no longer observed in the PA B-mode images, indicating that the degradation process was complete between 7 and 14 days (Figure S6).

The angiogenesis induced by the implanted SCAI patches over time was photoacoustically recorded (Fig. 5(C) and Figure S7). After 14 days of implantation, multiple sprouting of microvascular structures was observed at the surface of the SCAI patch implanted site, whereas no significant changes of microvascular structures were revealed in the non-treatment group. The newly-formed blood vessels with a diameter of 50 μm or smaller were highly observed on day 14 in the SCAI patch group due to the synergistic angiogenic efficacy of released VEGF and HGF [62]. Meanwhile, the original blood vessels, partially covered with the newly generated ves-

sels, could be identified in the magnified image (exhibited by inset images). The hidden original vessels were clearly visible in the B-mode images from the C1 and C2 regions of image in Fig. 5(C), highlighted with white dotted line in the MAP images (Fig. 5(D)). The original and newly generated vessels are outlined with yellow and white curves, respectively. We confirmed that during the angiogenesis process induced by SCAI patches, the existing blood vessels remain intact.

Additionally, quantitative analyses of the density for the newly formed blood vessels were performed by comparing the density of blood vessels (Fig. 5(E)). The densities of blood vessels were determined as the ratio of area for the blood vessels smaller than 50 μm in diameter to the implanted surface area. The densities obtained before and 14 days after patch implantation were compared. The densities were found as 0.0609 ± 0.0052 mm^2 mm^{-2} and 0.1999 ± 0.0239 mm^2 mm^{-2} on day 0 and day 14, respectively. The densities were increased approximately 3.3 times in 14 days after SCAI patches implantation The results suggested the efficacy of the SCAI patch to promote cerebral angiogenesis.

The histological evaluations were also conducted to verify angiogenic efficacy of the SCAI patch, which revealed similar results as the PAM imaging experiments. With the brains of sacrificed rats 14 days after SCAI patch implantation, we observed that the large blood vessels were remained, capable of supplying of blood to the surrounding tissues at the patch implanted site (Fig. 5(F)). Meanwhile, we could not observe the hydrogel SCAI patch, since the patch was completely degraded after 14 days. Numerous capillaries with various diameters and lengths were also highly observed in the group with implanted SCAI patch, indicated by black arrows. Some of the blood vessels were sprouted from the original large vessel, which is an obvious evidence of angiogenesis (shown by blue arrow). In contrast, the non-treatment group did not show any sprouted blood vessels. We also cross-validated the angiogenic effects of the implanted patch using immunohistochemistry (IHC) against the blood vessel specific antibody and observed similar trends to that of the hematoxylin and eosin (H&E) staining results (indicated by black arrows). These IHC images were obtained through cutting the brain longitudinally with respect to the patch implantation site 14 days after the patch was implanted. The blood vessels were observed even to a depth of approximately 100 μm under the influence of the growth factors released from the implanted SCAI patch. Furthermore, the degree of angiogenesis was quantified with counting the number of blood vessels per unit area (1 mm^2). The numbers of blood vessels were revealed 167 ± 13 for the SCAI patch implanted group and 29 ± 5 for the non-treatment group. This observation indicates 5.76 times greater number of vessels in 1 mm^2 in the SCAI patch implanted group (Fig. 5(G)). Taken together, we concluded that the SCAI patch clearly promoted angiogenesis and neovascularization, maintaining its efficacy up to 14 days *in vivo*.

4. Discussion

In this study, we developed a flexible patch-type drug delivery system with capability to provide the desired release profiles of dual angiogenic factors to promote cerebral angiogenesis at the brain site. The core competencies of the developed SCAI patch include: (1) Controllability of the release profiles with varying the density of the chemical crosslinking between the methacrylate and the amine functional groups in the developed HAVEM inks; (2) sequential and sustained release of the factors via spatiotemporally compartmentalization to localize these angiogenic GFs using 3D printing technology.

The conventional biofabrication strategies (e.g., mold casting, gas foaming, and freeze-drying) have been widely applied for producing biomaterials-based drug delivery systems; however, these methods inevitably entail multiple and complex processes [52,53]. Moreover, these approaches may require the additional processes for the treatment of cytotoxic solutions or managing the harsh environmental factors (e.g., pH, temperature), which are highly critical to decrease the stability of protein-based drugs [52]. On the other hand, application of 3D printing technology allowed us to fabricate spatially separated inner and outer layers in a single-step process without any physical interruptions. This method is beneficial to reduce the overall fabricating time and provide proper conditions to maintain higher bioactivity of GFs [52]. Furthermore, the developed HAVEM ink is also able to contribute to maintain bioactivity of GFs, because the inks were formed under mild crosslinking conditions that do not require catalysts as well as chemically active substances, including toxic radicals were not formed during reaction.

The patch with spatiotemporally compartmentalized dual angiogenic factors provides significant impacts on inducing the neovascularization in the brain. We investigated *in vivo* angiogenic efficacy using the OR-PAM system to monitor the time-dependent changes of microvasculature in the cerebral cortex of rats for 14 days. This imaging modality is an agent-free vascular imaging method, obtaining vascular images through measurement of the generated PA waves by intrinsic red blood cells from the vasculature. Therefore, we could identify the functional and integrated newly formed vessels with a more effective non-invasive way compared with the conventional vascular imaging modalities [63].

The SCAI patch may also serve as a reliable guidance for further investigations of its neoangiogenic potentials in the brain ischemic areas. We will conduct PK/PD studies *in vivo* for further validation of SCAI patches. The developed patch system of slow-releasing angiogenic GFs will likely expand a therapeutic window to target challenging and intractable chronic cerebral ischemic diseases, such as moyamoya disease. This disease is a progressive occlusive arteriopathy characterized by occlusion of the internal carotid artery and its branches. Surgical intervention (i.e., direct anastomosis, indirect revascularization) is the standard therapy for patients with moyamoya disease; however, there is no choice for pediatric patients because of the small caliber of their superficial temporal artery (STA) for direct anastomosis to the middle cerebral artery. Therefore, indirect revascularization strategies (i.e. encephaloduroarteriosynangiosis (EDAS)) are widely accepted as the treatment choice in children with moyamoya disease. The efficacy of this indirect surgery is usually due to the higher levels of GFs in the cerebrospinal fluid and an age-associated angiogenic capability [64,65]. The developed SCAI patch may have beneficial effects to promote the synangiogenesis between the STA and the dural blood vessels as well as neovascularization by simply placing the SCAI patch nearby the area after the indirect surgery or by replacing the omental and the dural flaps as an accelerator to increase the surface area of contact between the vascularized outer layer and the ischemic brain.

Furthermore, we will apply the developed SCAI patch to an aged brain in our future work. Through this, we could verify the pattern of angiogenesis induced in the aged brain and how it is the same as or different from that in the young brain [66]. In particular, it will be possible to determine how the angiogenesis pattern changes by specific external factors (e.g., stroke). In addition, the patch developed with this 3D printing technology could be used to improve long-distance nerve guide regeneration strategies [67]. 3D printing in peripheral nerve regeneration is an automated fabrication process with versatility of drugs delivery (potentially customized their diameter and length specifically for the patient) and of structures within the nerve guide that significantly outperform the nerve autograft over large gap injuries.

5. Conclusions

In summary, the results from this study highlight the outstanding potential of the spatiotemporally compartmentalized cerebral angiogenesis inducing patch using the HAVEM ink crosslinked via aza-Michael addition reaction. To the best of our knowledge, this is the first successful study using the crosslinking chemistry of aza-Michael addition reaction to synthesize dECM-based hybrid inks for effective production of complex patch-type constructs with enhanced printability. The hybrid ink with higher crosslinking density can effectively decrease the releasing rate of GFs since the higher chemical bond density affects to have smaller pore areas. Moreover, 3D printing technique enables to compartment the laden GFs in SCAI patches, which induces sustained and sequential release of GFs. Hence, the fabricated SCAI patches within these strategies are capable to deliver dual angiogenic GFs for a sustained and sequential manners to induce angiogenesis. Consequently, this drug delivery platform may effectively overcome the challenges of current long-term drug delivery approaches. The composition of the patch, consisting of VdECM and HA, is highly tissue specific material that provides soft and flexible properties with fabrication versatility [57]. The developed SCAI patch may offer a promising alternative therapeutic approach to effectively induce neovascularization in diverse acute or chronic cerebral ischemic diseases. Furthermore, the patch may also serve as promising guidance for the universal dosage-regulating local drug delivery approach by simply applying various alternative drugs or fabricating additional layers to laden multiple drugs of patch which may be applicable for further clinical perspective with ischemic heart diseases, diabetes, and even vaccines for COVID-19.

Author contributions

S.H. Hwang, C. Kim, S.H. Paek, and J. Jang initiated, conceptualized, analyzed, interpreted the data and wrote the manuscript. S.H. Hwang, J. Kim, C. Heo, H. Kim, S.-H. Lee, and J. Jang conducted experiments and visualized the data. S.H. Hwang and J. Kim wrote the manuscript and S.H. Hwang, J. Kim, H. Kim, H.W. Park, M.S. Heo, and H.E. Moon revised the manuscript. C. Kim, S.H. Paek, and J. Jang supervised the work, provided financial and administrative support, and revised the manuscript.

Funding

This work was supported by the National Research Foundation of Korea (NRF) grant funded by the Korea government (MSIT) (2021R1A2C2004981, NRF2019R1A2C2006269, and NRF2017M3C7A1047392). This work was also supported by Basic Science Research Program through the National Research Foundation of Korea (NRF) funded by the Ministry of Education (2020R1A6A1A03047902). This work was partly supported by the Bio & Medical Technology Development Program of the National Research Foundation (2015M3C7A1028926 and 2020M3A9G8022029); the Korea Research Institute of Bioscience and Biotechnology (KRIBB) Research Initiative Program (KGM456212109816); and Electronics and Telecommunications Research Institute (ETRI) grant funded by the Korea government (21YB1500) to S.H. Paek.

Data availability statement

The raw data required to reproduce these findings are available from the corresponding author, J.J, upon reasonable request.

Declaration of Competing Interest

J.J. owns equity in EdmicBio Inc. and holds stock options in T&R Biofab Inc. C.K. has financial interests in OPTICHO Inc. which, however, did not support this work. All other authors declare they have no competing interests.

Acknowledgements

S.H. Hwang and J. Kim contributed equally to this work. The authors thank Prof. Dong-Woo Cho, Mr. Jeongsik Kong, and Mr. Jae Yun Kim at POSTECH for instrumental discussions and directions for this work.

Supplementary materials

Supplementary material associated with this article can be found, in the online version, at doi:10.1016/j.actbio.2022.11.050.

References

[1] K.H. Plate, Mechanisms of angiogenesis in the brain, J. Neuropathol. Exp. Neurol. 58 (4) (1999) 313–320.
[2] Y. Fan, G.-Y. Yang, Therapeutic angiogenesis for brain ischemia: a brief review, J. Neuroimmune Pharmacol. 2 (3) (2007) 284–289.
[3] J.D. Easton, J.L. Saver, G.W. Albers, M.J. Alberts, S. Chaturvedi, E. Feldmann, T.S. Hatsukami, R.T. Higashida, S.C. Johnston, C.S. Kidwell, Definition and evaluation of transient ischemic attack: a scientific statement for healthcare professionals from the American Heart Association/American Stroke Association Stroke Council; Council on Cardiovascular Surgery and Anesthesia; Council on Cardiovascular Radiology and Intervention; Council on Cardiovascular Nursing; and the Interdisciplinary Council on Peripheral Vascular Disease: the American Academy of Neurology affirms the value of this statement as an educational tool for neurologists, Stroke 40 (6) (2009) 2276–2293.
[4] P.M. Rothwell, C.P. Warlow, Timing of TIAs preceding stroke: time window for prevention is very short, Neurology 64 (5) (2005) 817–820.
[5] G.J. Hankey, C.P. Warlow, Treatment and secondary prevention of stroke: evidence, costs, and effects on individuals and populations, Lancet North Am. Ed. 354 (9188) (1999) 1457–1463.
[6] S.B. Coutts, Diagnosis and management of transient ischemic attack, CONTINUUM: Lifelong Learn. Neurol. 23 (1) (2017) 82.
[7] H.V. Gupta, A.M. Farrell, M.K. Mittal, Transient ischemic attacks: predictability of future ischemic stroke or transient ischemic attack events, Ther. Clin. Risk Manage. 10 (2014) 27.
[8] S. Prabhakaran, A.J. Silver, L. Warrior, B. McClenathan, V.H. Lee, Misdiagnosis of transient ischemic attacks in the emergency room, Cerebrovasc. Dis. 26 (6) (2008) 630–635.
[9] P.C. Lavallée, E. Meseguer, H. Abboud, L. Cabrejo, J.-M. Olivot, O. Simon, M. Mazighi, C. Nifle, P. Niclot, B. Lapergue, A transient ischaemic attack clinic with round-the-clock access (SOS-TIA): feasibility and effects, Lancet Neurol. 6 (11) (2007) 953–960.
[10] W.F. Fearon, F.M. Zimmermann, B. De Bruyne, Z. Piroth, A.H. van Straten, L. Szekely, G. Davidavičius, G. Kalinauskas, S. Mansour, R. Kharbanda, Fractional flow reserve–guided PCI as compared with coronary bypass surgery, N. Engl. J. Med. (2021).
[11] Y. Brudno, A.B. Ennett-Shepard, R.R. Chen, M. Aizenberg, D.J. Mooney, Enhancing microvascular formation and vessel maturation through temporal control over multiple pro-angiogenic and pro-maturation factors, Biomaterials 34 (36) (2013) 9201–9209.
[12] H. Beck, K.H. Plate, Angiogenesis after cerebral ischemia 117 (5) (2009) 481–496 Acta neuropathologica.
[13] J.M. Rosenstein, N. Mani, W.F. Silverman, J.M. Krum, Patterns of brain angiogenesis after vascular endothelial growth factor administration *in vitro* and *in vivo*, Proc. Natl. Acad. Sci. 95 (12) (1998) 7086–7091.
[14] H. Chu, Y. Wang, Therapeutic angiogenesis: controlled delivery of angiogenic factors, Ther. Deliv. 3 (6) (2012) 693–714.
[15] T.D. Henry, Therapeutic angiogenesis, BMJ 318 (7197) (1999) 1536–1539.
[16] A. Fallah, A. Sadeghinia, H. Kahroba, A. Samadi, H.R. Heidari, B. Bradaran, S. Zeinali, O. Molavi, Therapeutic targeting of angiogenesis molecular pathways in angiogenesis-dependent diseases, Biomed. Pharmacother. 110 (2019) 775–785.
[17] H.K. Awada, N.R. Johnson, Y. Wang, Sequential delivery of angiogenic growth factors improves revascularization and heart function after myocardial infarction, J. Controlled Release 207 (2015) 7–17.
[18] X. Xin, S. Yang, G. Ingle, C. Zlot, L. Rangell, J. Kowalski, R. Schwall, N. Ferrara, M.E. Gerritsen, Hepatocyte growth factor enhances vascular endothelial growth factor-induced angiogenesis *in vitro* and *in vivo*, Am. J. Pathol. 158 (3) (2001) 1111–1120.

[19] C. Borselli, H. Storrie, F. Benesch-Lee, D. Shvartsman, C. Cezar, J.W. Lichtman, H.H. Vandenburgh, D.J. Mooney, Functional muscle regeneration with combined delivery of angiogenesis and myogenesis factors, Proc. Natl. Acad. Sci. 107 (8) (2010) 3287–3292.
[20] R. Cao, E. Bråkenhielm, R. Pawliuk, D. Wariaro, M.J. Post, E. Wahlberg, P. Leboulch, Y. Cao, Angiogenic synergism, vascular stability and improvement of hind-limb ischemia by a combination of PDGF-BB and FGF-2, Nat. Med. 9 (5) (2003) 604–613.
[21] T.P. Richardson, M.C. Peters, A.B. Ennett, D.J. Mooney, Polymeric system for dual growth factor delivery, Nat. Biotechnol. 19 (11) (2001) 1029–1034.
[22] R. Chapanian, B. Amsden, Combined and sequential delivery of bioactive VEGF165 and HGF from poly (trimethylene carbonate) based photo-to-cross-linked elastomers, J. Controlled Release 143 (1) (2010) 53–63.
[23] P.I. Makarevich, K.V. Dergilev, Z.I. Tsokolaeva, M.A. Boldyreva, E.K. Shevchenko, E.V. Gluhanyuk, J.O. Gallinger, M.Y. Menshikov, Y.V. Parfyonova, Angiogenic and pleiotropic effects of VEGF165 and HGF combined gene therapy in a rat model of myocardial infarction, PLoS One 13 (5) (2018) e0197566.
[24] M.E. Gerritsen, HGF and VEGF: a dynamic duo, Circ. Res. 96 (3) (2005) 272–273.
[25] W.B. Liechty, D.R. Kryscio, B.V. Slaughter, N.A. Peppas, Polymers for drug delivery systems, Annu. Rev. Chem. Biomol. Eng. 1 (2010) 149–173.
[26] T.R. Hoare, D.S. Kohane, Hydrogels in drug delivery: progress and challenges, Polymer 49 (8) (2008) 1993–2007.
[27] R. Langer, Drug delivery and targeting, Nature 392 (6679) (1998) 5–10 Suppl.
[28] J. Li, D.J. Mooney, Designing hydrogels for controlled drug delivery, Nat. Rev. Mater. 1 (12) (2016) 1–17.
[29] Y. Qiu, K. Park, Environment-sensitive hydrogels for drug delivery, Adv. Drug. Deliv. Rev. 53 (3) (2001) 321–339.
[30] F. Pati, J. Jang, D.-.H. Ha, S.W. Kim, J.-.W. Rhie, J.-.H. Shim, D.-.H. Kim, D.-.W. Cho, Printing three-dimensional tissue analogues with decellularized extracellular matrix bioink, Nat. Commun. 5 (1) (2014) 1–11.
[31] B. Derby, Printing and prototyping of tissues and scaffolds, Science 338 (6109) (2012) 921–926.
[32] J. Leijten, J. Seo, K. Yue, G. Trujillo-de Santiago, A. Tamayol, G.U. Ruiz-Esparza, S.R. Shin, R. Sharifi, I. Noshadi, M.M. Álvarez, Spatially and temporally controlled hydrogels for tissue engineering, Mater. Sci. Eng. R. Rep. 119 (2017) 1–35.
[33] N. Liu, S. Huang, B. Yao, J. Xie, X. Wu, X. Fu, 3D bioprinting matrices with controlled pore structure and release function guide *in vitro* self-organization of sweat gland, Sci. Rep. 6 (1) (2016) 1–8.
[34] P.S. Gungor-Ozkerim, I. Inci, Y.S. Zhang, A. Khademhosseini, M.R. Dokmeci, Bioinks for 3D bioprinting: an overview, Biomater. Sci. 6 (5) (2018) 915–946.
[35] S. Young, M. Wong, Y. Tabata, A.G. Mikos, Gelatin as a delivery vehicle for the controlled release of bioactive molecules, J. Controlled Release 109 (1–3) (2005) 256–274.
[36] S. Rhee, J.L. Puetzer, B.N. Mason, C.A. Reinhart-King, L.J. Bonassar, 3D bioprinting of spatially heterogeneous collagen constructs for cartilage tissue engineering, ACS Biomater. Sci. Eng. 2 (10) (2016) 1800–1805.
[37] J. Lu, F. Guan, F. Cui, X. Sun, L. Zhao, Y. Wang, X. Wang, Enhanced angiogenesis by the hyaluronic acid hydrogels immobilized with a VEGF mimetic peptide in a traumatic brain injury model in rats, Regener. Biomater. 6 (6) (2019) 325–334.
[38] K. Nägga, O. Hansson, D. van Westen, L. Minthon, M. Wennström, Increased levels of hyaluronic acid in cerebrospinal fluid in patients with vascular dementia, J. Alzheimers Dis. 42 (4) (2014) 1435–1441.
[39] J. Jang, H.-.J. Park, S.-.W. Kim, H. Kim, J.Y. Park, S.J. Na, H.J. Kim, M.N. Park, S.H. Choi, S.H. Park, 3D printed complex tissue construct using stem cell-laden decellularized extracellular matrix bioinks for cardiac repair, Biomaterials 112 (2017) 264–274.
[40] G. Gao, W. Park, B.S. Kim, M. Ahn, S. Chae, W.W. Cho, J. Kim, J.Y. Lee, J. Jang, D.W. Cho, Construction of a novel *in vitro* atherosclerotic model from geometry-tunable artery equivalents engineered via in-bath coaxial cell printing, Adv. Funct. Mater. 31 (10) (2021) 2008878.
[41] G. Gao, J.Y. Park, B.S. Kim, J. Jang, D.W. Cho, Coaxial cell printing of freestanding, perfusable, and functional *in vitro* vascular models for recapitulation of native vascular endothelium pathophysiology, Adv. Healthc. Mater. 7 (23) (2018) 1801102.
[42] M.T. Wolf, K.A. Daly, E.P. Brennan-Pierce, S.A. Johnson, C.A. Carruthers, A. D'Amore, S.P. Nagarkar, S.S. Velankar, S.F. Badylak, A hydrogel derived from decellularized dermal extracellular matrix, Biomaterials 33 (29) (2012) 7028–7038.
[43] D.A. Taylor, L.C. Sampaio, Z. Ferdous, A.S. Gobin, L.J. Taite, Decellularized matrices in regenerative medicine, Acta Biomater. 74 (2018) 74–89.
[44] S.-.W. Cho, S.M. Park, B. Park, T.G. Lee, B.-.M. Kim, C. Kim, J. Kim, S.-.W. Lee, C.-.S. Kim, High-speed photoacoustic microscopy: a review dedicated on light sources, J. Photoacoust. (2021) 100291.
[45] J. Ahn, J.Y. Kim, W. Choi, C. Kim, High-resolution functional photoacoustic monitoring of vascular dynamics in human fingers, J. Photoacoust. 23 (2021) 100282.
[46] J. Park, B. Park, T.Y. Kim, S. Jung, W.J. Choi, J. Ahn, D.H. Yoon, J. Kim, S. Jeon, D. Lee, Quadruple ultrasound, photoacoustic, optical coherence, and fluorescence fusion imaging with a transparent ultrasound transducer, Proc. Natl. Acad. Sci. 118 (11) (2021).
[47] S. Cho, J. Baik, R. Managuli, C. Kim, 3D PHOVIS: 3D photoacoustic visualization studio, J. Photoacoust. 18 (2020) 100168.
[48] J.W. Baik, J.Y. Kim, S. Cho, S. Choi, J. Kim, C. Kim, Super wide-field photoacoustic microscopy of animals and humans *in vivo*, IEEE Trans. Med. Imaging 39 (4) (2019) 975–984.
[49] X. Cai, Y. Zhang, L. Li, S.-.W. Choi, M.R. MacEwan, J. Yao, C. Kim, Y. Xia, L.V. Wang, Investigation of neovascularization in three-dimensional porous scaffolds *in vivo* by a combination of multiscale photoacoustic microscopy and optical coherence tomography, Tissue Eng. Part C Methods 19 (3) (2013) 196–204.
[50] J.Y. Kim, C. Lee, K. Park, G. Lim, C. Kim, Fast optical-resolution photoacoustic microscopy using a 2-axis water-proofing MEMS scanner, Sci. Rep. 5 (1) (2015) 1–5.
[51] C. Heo, H. Park, Y.-.T. Kim, E. Baeg, Y.H. Kim, S.-.G. Kim, M. Suh, A soft, transparent, freely accessible cranial window for chronic imaging and electrophysiology, Sci. Rep. 6 (1) (2016) 1–11.
[52] J. Kim, J.Y. Kim, S. Jeon, J.W. Baik, S.H. Cho, C. Kim, Super-resolution localization photoacoustic microscopy using intrinsic red blood cells as contrast absorbers, Light: Sci. Appl. 8 (1) (2019) 1–11.
[53] S. Jeon, J. Kim, D. Lee, J.W. Baik, C. Kim, Review on practical photoacoustic microscopy, J. Photoacoust. 15 (2019) 100141.
[54] Z. Wang, A.C. Bovik, H.R. Sheikh, E.P. Simoncelli, Image quality assessment: from error visibility to structural similarity, IEEE Trans. Image Process. 13 (4) (2004) 600–612.
[55] A.F. Frangi, W.J. Niessen, K.L. Vincken, M.A. Viergever, in: Multiscale vessel enhancement filtering, International conference on medical image computing and computer-assisted intervention, Springer, 1998, pp. 130–137.
[56] M.T. Poldervaart, B. Goversen, M. De Ruijter, A. Abbadessa, F.P. Melchels, F.C. Öner, W.J. Dhert, T. Vermonden, J. Alblas, 3D bioprinting of methacrylated hyaluronic acid (MeHA) hydrogel with intrinsic osteogenicity, PLoS One 12 (6) (2017) e0177628.
[57] B.S. Kim, S. Das, J. Jang, D.-.W. Cho, Decellularized extracellular matrix-based bioinks for engineering tissue-and organ-specific microenvironments, Chem. Rev. 120 (19) (2020) 10608–10661.
[58] T. Wooster, S. Acquistapace, C. Mettraux, L. Donato, B. Dekkers, Hierarchically structured phase separated biopolymer hydrogels create tailorable delayed burst release during gastrointestinal digestion, J. Colloid Interface Sci. 553 (2019) 308–319.
[59] W. McIntosh Ambrose, A. Salahuddin, S. So, S. Ng, S. Ponce Márquez, T. Takezawa, O. Schein, J. Elisseeff, Collagen vitrigel membranes for the *in vitro* reconstruction of separate corneal epithelial, stromal, and endothelial cell layers, J. Biomed. Mater. Res. Part B: Appl. Biomater.: Off. J. Soc. Biomater. Japanese Soc. Biomater. Austr. Soc. Biomater. Korean Soc. Biomater. 90 (2) (2009) 818–831.
[60] X. Calderón-Colón, Z. Xia, J.L. Breidenich, D.G. Mulreany, Q. Guo, O.M. Uy, J.E. Tiffany, D.E. Freund, R.L. McCally, O.D. Schein, Structure and properties of collagen vitrigel membranes for ocular repair and regeneration applications, Biomaterials 33 (33) (2012) 8286–8295.
[61] N. Peppas, P. Bures, W. Leobandung, H. Ichikawa, Hydrogels in pharmaceutical formulations, Eur. J. Pharm. Biopharm. 50 (1) (2000) 27–46.
[62] A.C. Ngai, H.R. Winn, Modulation of cerebral arteriolar diameter by intraluminal flow and pressure, Circ. Res. 77 (4) (1995) 832–840.
[63] J. Yao, L.V. Wang, Photoacoustic microscopy, Laser Photonics Rev. 7 (5) (2013) 758–778.
[64] S. Kuroda, K. Houkin, Moyamoya disease: current concepts and future perspectives, Lancet Neurol. 7 (11) (2008) 1056–1066.
[65] R.M. Scott, E.R. Smith, Moyamoya disease and moyamoya syndrome, N. Engl. J. Med. 360 (12) (2009) 1226–1237.
[66] A.M. Buga, C. Margaritescu, C.J. Scholz, E. Radu, C. Zelenak, A. Popa-Wagner, Transcriptomics of post-stroke angiogenesis in the aged brain, Front. Aging Neurosci. 6 (2014) 44.
[67] E.B. Petcu, R. Midha, E. McColl, A. Popa-Wagner, T.V. Chirila, P.D. Dalton, 3D printing strategies for peripheral nerve regeneration, Biofabrication 10 (3) (2018) 032001.